



Contents lists available at SciVerse ScienceDirect

Acta Biomaterialia

journal homepage: www.elsevier.com/locate/actabiomat

A surface-eroding poly(1,3-trimethylene carbonate) coating for fully biodegradable magnesium-based stent applications: Toward better biofunction, biodegradation and biocompatibility ☆

Juan Wang^{a,b,c}, Yonghui He^{a,b}, Manfred F. Maitz^{a,d}, Boyce Collins^c, Kaiqin Xiong^{a,b}, Lisha Guo^{a,b}, Yeoheung Yun^c, Guojiang Wan^{a,b,*}, Nan Huang^{a,b,*}

^a Key Laboratory of Advanced Technologies of Materials, Ministry of Education, School of Materials Science and Engineering, Southwest Jiaotong University, Chengdu 610031, China

^b The Institute of Biomaterials and Surface Engineering, School of Materials Science and Engineering, Southwest Jiaotong University, Chengdu 610031, China

^c National Science Foundation Engineering Research Center for Revolutionizing Metallic Biomaterials, North Carolina A & T State University, Greensboro, NC 27411, USA

^d Leibniz Institute of Polymer Research Dresden, Max Bergmann Center of Biomaterials Dresden, Dresden 01069, Germany

ARTICLE INFO

Article history:

Available online xxxxx

Keywords:

Surface-eroding coating
Magnesium
Poly(1,3-trimethylene carbonate)
Biodegradable stent
Biocompatibility

ABSTRACT

Biodegradable magnesium-based materials have a high potential for cardiovascular stent applications; however, there exist concerns on corrosion control and biocompatibility. A surface-eroding coating of poly(1,3-trimethylene carbonate) (PTMC) on magnesium (Mg) alloy was studied, and its dynamic degradation behavior, electrochemical corrosion, hemocompatibility and histocompatibility were investigated. The PTMC coating effectively protected the corrosion of the Mg alloy in the dynamic degradation test. The corrosion current density of the PTMC-coated alloy reduced by three orders and one order of magnitude compared to bare and poly(ϵ -caprolactone) (PCL)-coated Mg alloy, respectively. Static and dynamic blood tests in vitro indicated that significantly fewer platelets were adherent and activated, and fewer erythrocytes attached on the PTMC-coated surface and showed less hemolysis than on the controls. The PTMC coating after 16 weeks' subcutaneous implantation in rats maintained ~55% of its original thickness and presented a homogeneously flat surface demonstrating surface erosion, in contrast to the PCL coated control, which exhibited non-uniform bulk erosion. The Mg alloy coated with PTMC showed less volume reduction and fewer corrosion products as compared to the controls after 52 weeks in vivo. Excessive inflammation, necrosis and hydrogen gas accumulation were not observed. The homogeneous surface erosion of the PTMC coating from exterior to interior (surface-eroding behavior) and its charge neutral degradation products contribute to its excellent protective performance. It is concluded that PTMC is a promising candidate for a surface-eroding coating applied to Mg-based implants.

© 2013 Acta Materialia Inc. Published by Elsevier Ltd. All rights reserved.

1. Introduction

Most current conventional bare metal stents and drug eluting stents are made of non-degradable metals and polymers, which may negatively interact with the surrounding tissues in chronic pathological response stage [1–3]. These side-effects include long-term endothelial dysfunction, delayed re-endothelialization, late thrombosis, permanent physical irritation, toxic metal ion release, local chronic inflammation and, importantly, non-permissive or disadvantageous properties for later surgical revascularization

[4–6]. One remedy to these complications is the development of more biocompatible and degradable stents. Ideally, implanted stents are expected to degrade or be absorbed after they fulfill the aim of strutting the stenosed vessel and repairing the damaged tissue [7–9].

In the past decade, magnesium-based materials have received considerable attention as a promising candidate for a new generation of biodegradable stent materials, owing to their in vivo degradation characteristics [10], non-toxicity [11], excellent mechanical properties and benign manufacturing performance [12], as well as abundant availability of the raw material. However, the major obstacle for clinical applications of Mg-based materials is controlling the high corrosion rate [13,14]. Negative effects of fast degradation include the formation of hydrogen bubbles [15,16], hemolytic reactions due to high local pH value [17] and a premature loss of mechanical strength of the stent during the period of time required for healing.

☆ Part of the Biodegradable Metals Conference 2012 Special Issue, edited by Professor Frank Witte and Professor Diego Mantovani.

* Corresponding authors. Tel./fax: +86 28 87600625 (Nan Huang). Tel.: +86 28 87634146; fax: +86 28 87600625 (Guojiang Wan).

E-mail addresses: guojiang.wan@home.swjtu.edu.cn (G. Wan), nhuang@263.net (N. Huang).

Many efforts have been devoted to increase the corrosion resistance of the magnesium via surface modification [13,18,19] including microarc oxidation [20–22], anodization treatment [23], steam treatment [24], alkaline heat treatment [25], fluoride treatment [26,27], electro-deposition [28], phosphating treatment [29], laser shock peening [30], ion implantation [31], physical vapor deposition [32] and polymer coating [33,34]. Comparatively, biodegradable polymer coatings may be superior to others in many aspects [35]. However, coatings with suitable durability and good biocompatibility still have not been achieved yet, and are highly desirable for the clinical requirements of Mg-based cardiovascular stents. Recent studies have shown that some biodegradable polymer coating candidates, e.g. PLA, PCL and PGA, undermine rather than enhance corrosion resistance of Mg-based metal [36] owing to a bulk erosion behavior of these polymers [37] and acidic product generation upon degradation of these coatings [38]. Therefore, a surface eroding polymer exhibiting homogeneous erosion from exterior to interior with neutral degradation products may be a more suitable coating for Mg-based implants.

In this study, a surface-eroding polymer, PTMC, is carefully screened as a coating material for Mg alloys. Their corresponding degradation behavior as well as blood and tissue compatibility are systematically investigated. The degradation performance and mechanism are also discussed. The feasibility to use the PTMC-coated Mg alloy as cardiovascular stent is also evaluated.

2. Experimental

2.1. Preparation of material and coating

High-purity Mg alloy (MgZnMn) with 1 wt.% zinc (Zn) and 0.2 wt.% manganese (Mn) was prepared by melting and extruding to rod shape. Strip specimens 15 mm in length, 5 mm in width and 1.5 mm in height were used for in vitro degradation tests. Disk specimens with a diameter of 10 mm and a height of 1.5 mm were prepared for in vitro hemocompatibility evaluations. Wire specimens with a diameter of 1 mm and a length of 10 mm were applied for the in vivo studies. The MgZnMn specimens were first ground with SiC paper progressively up to 4000 grits and then mechanically polished with 1 μm diamond cloth followed by ultrasonic cleaning with acetone and ethanol, and dried at room temperature. The morphology of the specimen after polishing was examined by a field emission scanning electron microscope (FE-SEM, JSM-7001F, Japan).

PTMC $(-(\text{COOCH}_2\text{CH}_2\text{CH}_2\text{O})_n-)$ and PCL $(-(\text{COOCH}_2\text{CH}_2\text{CH}_2\text{CH}_2\text{CH}_2)_n-)$ with an average molecular weight of $\sim 500,000 \text{ g mol}^{-1}$ and $\sim 100,000 \text{ g mol}^{-1}$, respectively (Jinan Daigang Biomaterial Co., Ltd, China), were dissolved in dichloromethane (analytical grade) at a concentration of 1 wt.%. The polymer coatings on the alloy were fabricated via evaporation of the organic solvent from the respective coating solution. In the evaporation process, the solvent volatilization rate of 2 ml h^{-1} and temperature of 20°C were maintained for 24 h, thereby standardizing the thickness, homogeneity and adhesiveness of the coating. Uncoated and PCL-coated MgZnMn specimens were treated as controls. Surface morphology and the thicknesses of the polymer coating were observed by FE-SEM imaging.

2.2. In vitro degradation tests

Dynamic degradation tests and electrochemical corrosion measurements were performed in modified simulated body fluid (m-SBF) for evaluating degradation properties of the uncoated, PCL-coated and PTMC-coated MgZnMn alloy.

2.2.1. Dynamic degradation test

Dynamic degradation tests were conducted on a platform designed to mimic the environment encountered by stents in coronary arteries with a constant laminar flow [39]. m-SBF was chosen as a pseudo-physiological solution due to its stability and similar ion composition as human blood plasma [39]. Benzyl-penicillin sodium and streptomycin sulfate were added to m-SBF to inhibit the growth of bacteria. The m-SBF volume was kept at 300 ml. The pH value of the solution was adjusted to $7.4 \pm 0.2^\circ\text{C}$ prior to the test. The shear stress applied on the inner surface of the specimen was controlled to 0.68 Pa by modifying the flow rate of solution according to the following formula [40]:

$$\tau = 32\eta Q / (\pi D^3) \quad (1)$$

where τ is shear stress (0.68 Pa), η is liquid viscosity (3.5 mPa s), Q (65 ml min^{-1}) is the flux of the solution and D (3.8 mm) is the diameter of the lumen of the specimen.

During the dynamic degradation experiment, specimens were taken from the platform at set intervals and their mass was determined after drying in a vacuum oven at 37°C for 2 h. The corresponding pH value of the solution was recorded by a PHS-3C pH meter (Lei-ci, China). The concentration of Mg^{2+} in the solution was measured by inductively coupled plasma atomic emission spectrometry (AA800, PE, USA) and corrected for subtraction of the initial concentration of Mg^{2+} in m-SBF. Representative surface and cross-section morphologies and the coating thickness of the specimens were observed by FE-SEM. Those specimens for cross-section observation were brittle-fractured by immersing into liquid nitrogen. In addition, the surface chemical compositions of PTMC-coated MgZnMn subject to 30-day degradation tests were measured by X-ray photoelectron spectroscopy (XPS; XSAM800, Kratos Ltd, UK). The instrument was equipped with a monochromatic Al K_{α} (1486.6 eV) X-ray source operated at $12 \text{ kV} \times 15 \text{ mA}$ at a pressure of $2 \times 10^{-7} \text{ Pa}$. The C 1s peak (binding energy 284.8 eV) was used as a reference for calibration.

2.2.2. Electrochemical corrosion tests

Electrochemical corrosion tests were conducted on an electrochemical workstation (IM6, Zahner, Germany) with a three-electrode set-up: the specimen as working electrode, a platinum sheet as counter-electrode and a saturated calomel electrode (SCE) as reference electrode. 50 ml deoxygenated m-SBF incubated in a water bath at $37 \pm 0.2^\circ\text{C}$ served as electrolyte. The samples were sealed by silicon rubber with an uncovered working surface area of 0.75 cm^2 . Potentiodynamic polarization curves were scanned from -2 V to -1 V at a scan rate of 2 mV s^{-1} . The natural corrosion current (I_{corr}) and natural corrosion potential (E_{corr}) were determined by the Tafel extrapolation. The surface morphologies of the resultant specimens were observed by FE-SEM. The electrochemical impedance spectroscopy (EIS) measurement was done in the same set-up, with a scanning frequency range from 10^4 to 10^{-3} Hz , by a single AC mode of amplitude of 10 mV. EIS spectra were shown by Nyquist plots, and were quantitatively simulated using corresponding equivalent circuits.

2.3. In vitro hemocompatibility

Human whole blood was obtained from the central blood station of Chengdu, China according to standard legal protocols, and was used within 12 h after the donation. Citrate acid was added to the blood as an anticoagulant. The samples subjected to hemocompatibility tests included 316L stainless steel (316L SS), MgZnMn, PCL-coated MgZnMn and PTMC-coated MgZnMn. The number of parallel samples used for statistical count was not less than six.

2.3.1. Hemolysis

Blood solution was prepared by dilution of 4 ml of whole blood with 5 ml of 0.9% (w/v) sodium chloride solution. Every sample was immersed in 9.8 ml 0.9% (w/v) sodium chloride solution. Additionally, the 9.8 ml of 0.9% (w/v) sodium chloride solution (negative controls) and 9.8 ml double distilled water (positive controls) were prepared. All the samples were kept at 37 °C for 30 min and then mixed with 0.2 ml of the diluent blood at 37 °C for 60 min. All samples were centrifuged at 3000 rpm for 5 min. The supernatant of each sample was collected and absorbance was measured with a microplate reader at 540 nm to determine the y of cells undergoing hemolysis. Hemolysis ratio is calculated as follows:

$$R = (A - C1)/(C2 - C1)100\% \quad (2)$$

where R is the hemolysis ratio (%), A is the absorbance of the sample (%), $C1$ is the absorbance of the negative controls (%) and $C2$ is the absorbance of the positive control (%).

2.3.2. Static platelet incubation

Static platelet incubation was carried out to evaluate thrombogenicity of the samples and to examine the interaction between blood and the materials *in vitro*. In this test, platelet-rich plasma (PRP) was prepared by centrifuging human whole blood containing 3.8 wt.% citrate acid at 1,500 rpm for 15 min. Then 60 μ l of PRP was placed individually on top of each sample, and incubated at 37 °C for 2 h. After this, the samples were rinsed gently with phosphate buffer solution (PBS) three times, and 60 μ l of 2.5% glutaraldehyde solution was placed on the samples for 30 min. After rinsing with PBS three times, the samples were dehydrated sequentially in 50%, 75%, 90% and 100% ethanol solution. Finally, the samples were sputter-coated with gold, and imaged by FE-SEM.

2.3.3. Human whole blood adhesion experiments in flow chamber

Human whole blood adhesion tests were conducted in a closed flow chamber using 50 ml of the citrated whole blood (0.5 U ml⁻¹) *in vitro* (Supplementary materials, Fig. S1). All the samples were simultaneously exposed for 2 h to a flow of 65 ml min⁻¹ at a temperature of 37 °C. At the end of this test, the samples in the chamber were rinsed with PBS at a slow flow rate of 10 ml min⁻¹. Then the samples were removed and fixed in glutaraldehyde solution, and dehydrated in ethanol solutions as described above, and observed by FE-SEM.

2.4. *In vivo* animal study

To assess biointegration and the local effects of an implant in contact with living tissue, uncoated, PCL-coated and PTMC-coated MgZnMn wires were implanted subcutaneously in rats. The thicknesses of the polymer coatings were \sim 10 μ m. For pre-measuring the coating thickness, the PTMC- and PCL-coated MgZnMn wires for cross-section observation were brittle-fractured by immersing in liquid nitrogen. The formal specimens were sterilized by ultraviolet radiation prior to surgery. The number of parallel samples and rats used for statistical count was not less than three.

2.4.1. Surgery

The anesthetic, surgical and post-operative care protocols were taken from the international guidelines on animal experiments, and approved by the institutional committee for care and use of laboratory animals. Six three-month old female Sprague–Dawley rats weighing 250–275 g from the Laboratory Animal Unit of The University of Sichuan were used in this study. Each rat was anesthetized with 0.4 ml of pentobarbital sodium (30 mg ml⁻¹) by subcutaneous administration. After shaving and disinfection, subcutaneous pockets were made to three incisions on the back

of each rat. The PTMC-coated, PCL-coated and uncoated MgZnMn wires were placed in each pocket in the same rat. After 16 and 52 weeks, the implanted wires containing the surrounding tissue were harvested for analysis.

2.4.2. Morphology analysis of implants

The samples after 16 weeks' implantation were fixed in 10% buffered formalin for 3 days. A dehydrating process was performed using 70%, 80%, 90% and 100% ethanol, sequentially. The samples were immersed in each of the ethanol solutions for 12 h, and then brittle-fractured by immersion in liquid nitrogen. For one part of some samples, the tissue and polymer were removed to observe the corrosive surface of the metal wires. Another part was prepared for observation in the cross-section. The implants were sealed in the mixture of epoxy and hardener to protect corrosion products. The cross-sections of the samples were mechanically ground to 1200 grit on SiC paper. The fine polishing was done using 1 μ m diamond polishing paste. Samples were analyzed by X-ray computed tomography (GE Phoenix Nanotom-M™, GE Sensing & Inspection Technologies GmbH). In the nano-CT analysis for samples after 16 and 52 weeks' implantation, the two-dimensional (2-D) planes and the three-dimensional (3-D) models were reconstructed using the phoenix dataview software. The residual implant and corrosion product volumes were then analyzed using VG Studio Max software (v 2.1).

2.4.3. Histological evaluation

Samples were fixed in 10% buffered formalin, dehydrated in graded alcohol solutions and then embedded in paraffin. Histological sections (\sim 2 μ m) were stained with hematoxylin and eosin, mounted in permount solution, and imaged using an Olympus BX51, DP70 bright-field microscope.

2.5. Statistical analysis

The statistical significance of differences between groups was determined using one-way ANOVA followed by post-hoc analysis. Significance was established by a value of $p < 0.05$. Data are expressed as mean \pm standard deviation (SD).

3. Results

3.1. *In vitro* degradation tests

3.1.1. Dynamic degradation test

The dynamic degradation rate of the PTMC-coated MgZnMn was significantly lower than that of the uncoated and PCL-coated MgZnMn (Fig. 1). The PTMC-coated MgZnMn also exhibited the least increase of pH, Mg²⁺ release, and weight loss during the degradation, as compared with the uncoated and PCL-coated counterparts. After 30 days, the pH value of PTMC-coated MgZnMn solutions was still \sim 7.4 and the concentration of released Mg²⁺ did not exceed 3 mg l⁻¹ cm⁻² concomitant with a weight loss of 8 mg cm⁻². In contrast, the uncoated and PCL-coated MgZnMn showed a sharp increase of pH, significant Mg²⁺ release, and weight loss at early degradation stages and maintained a steady increase for all three values during the remainder of the experiment.

Corrosion morphologies for each type of samples at different intervals of the dynamic degradation process were presented (Fig. 2). The surface morphologies of all samples were fairly smooth and clean before and after coating (Fig. 2a, e and i). After 5 days of the degradation, the MgZnMn alloy surface was covered by a network of cracks (Fig. 2b), probably due to the corrosion along the grain boundaries. After 15 days, some corrosion products emerged on the cracked surface (Fig. 2c), and after 30 days, sheet

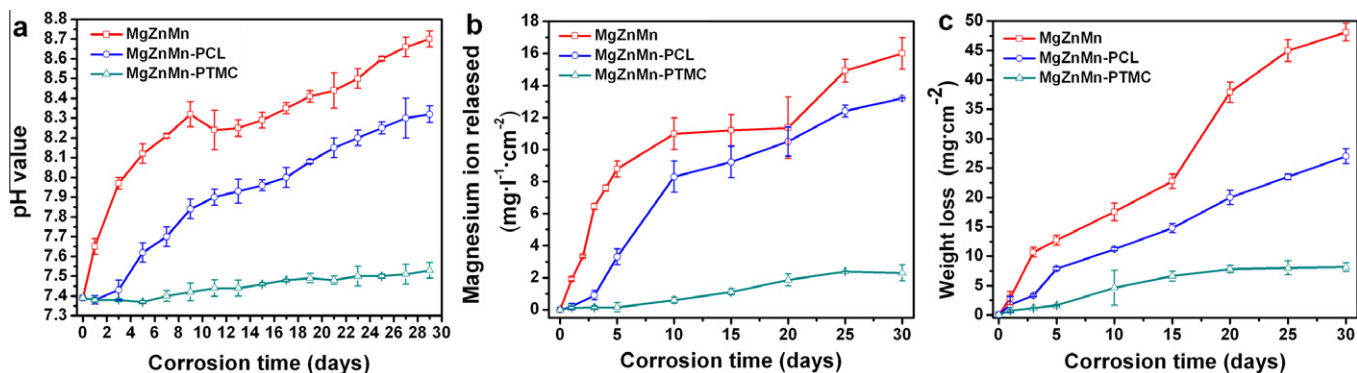


Fig. 1. Graphs charting the dynamic degradation of the uncoated, PCL-coated and PTMC-coated MgZnMn samples in m-SBF (37 ± 0.2 °C) as a function of time: (a) pH value of m-SBF; (b) the concentration of magnesium ion release; (c) weight loss of the specimens.

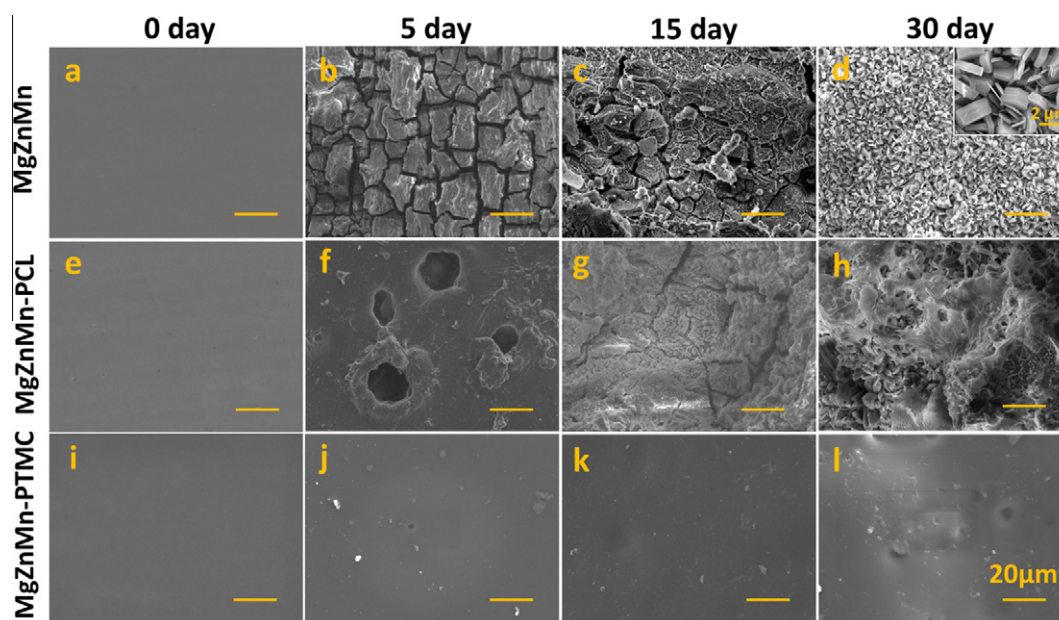


Fig. 2. Scanning electron micrographs of the surface morphologies of the uncoated, PCL-coated and PTMC-coated MgZnMn samples in dynamic m-SBF (37 ± 0.2 °C) after 0, 5, 15 and 30 days. Scale bar: 20 μm (unless otherwise stated).

crystal products fully covered the surface (Fig. 2d). The imaging of the PCL-coated MgZnMn after 5 days presented topography consistent with micropore eroding behavior (i.e. bulk erosion), as shown in Fig. 2f. After 15 days, the fragmentation of the polymer can be observed, and the MgZnMn substrate was partly exposed to the medium (Fig. 2g). After 30 days, the micrograph of residual polymers combined with the sheet crystal corrosion products of Mg alloys formed (Fig. 2h), indicating that the substrate had already been corroded. Significantly, the PTMC-coated MgZnMn sample still maintained a remarkably smooth and homogeneous surface after 30 days, with minimal damage phenomena found on the polymeric surface (Fig. 2j–l). Furthermore, no Mg peak was detected in XPS measurements (Supplementary materials, Fig. S2). These results confirm that the PTMC coating effectively protects the Mg alloy substrate during the 30 day exposure to flowing m-SBF solution.

Cross-section SEM images (Fig. 3) of the interface between the polymer coating and metal substrate at different intervals further illustrate the differences between the corrosion and protective properties of the two polymers. The thicknesses of the each coating were both initially 10 μm before degradation testing (Fig. 3a and d). After 10-days' degradation, the PCL coating presented typical

bulk-eroding characteristics with non-uniform degradation. Severe localized pitting corrosion of the exposed substrate (Fig. 3b in the frame) was observed. After 30 days, the interface between the polymer coating and metal substrate was less distinct. In contrast, the PTMC coating degradation fits well with a surface-eroding model from exterior to interior. Its thickness was uniformly thinned, and after 10 days, a homogeneous PTMC layer with a thickness of 8.5 μm remained on the intact substrate. Even after 30 days, the remaining PTMC coating had a thickness of ~ 5.5 μm and still fully enveloped the substrate, although underneath moderate substrate corrosion emerged. Thus, the surface-eroding degradation of PTMC coating presented a predictable constant erosion rate of ~ 4.5 μm per month in m-SBF under dynamic test conditions and significantly retarded the corrosion process of Mg alloy substrate.

3.1.2. Electrochemical corrosion measurements

The polarization curves of the PTMC-coated, PCL-coated and uncoated MgZnMn are shown in Fig. 4a. Natural corrosion current I_{corr} and natural corrosion potentials E_{corr} were determined by the Tafel extrapolation method [41], and the calculated values are listed in Table 1. I_{corr} of the PTMC-coated MgZnMn is over three orders of

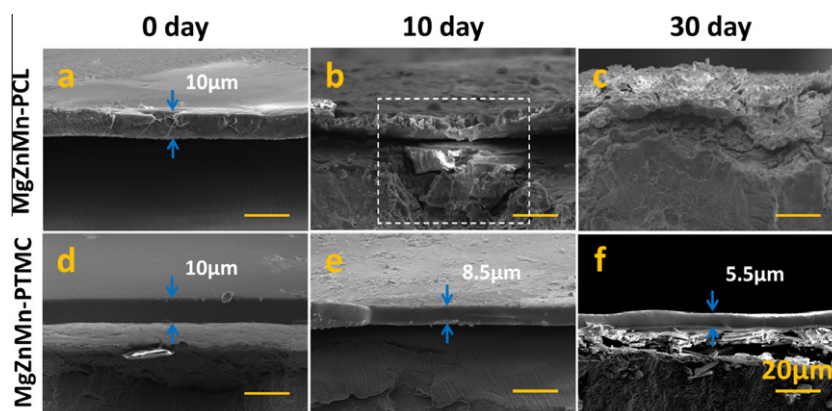


Fig. 3. Cross-section SEM morphologies of the PCL-coated and PTMC-coated MgZnMn samples in dynamic m-SBF (37 ± 0.2 °C) after 0, 10 and 30 days. The thickness of the polymer coating is indicated by the blue arrows. Scale bar: 20 μm .

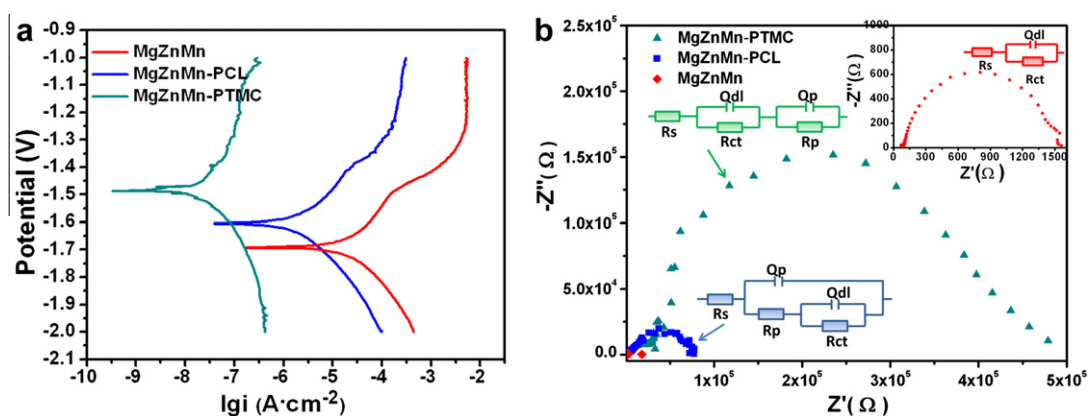


Fig. 4. Graphs of electrochemical measurements of the uncoated, PCL-coated and PTMC-coated MgZnMn samples in m-SBF (37 ± 0.2 °C): (a) polarization curves, (b) impedance spectrum and equivalent circuit model of the spectrum (inset is impedance spectrum at high frequencies).

Table 1

Electrochemical IE and EIS fitted parameters for bare, PCL-coated and PTMC-coated MgZnMn samples in m-SBF (37 ± 0.2 °C).

Sample	Parameters						
	I_{corr} (nA cm^{-2})	E_{corr} (V)	R_s (Ω)	R_{ct} (k Ω)	Q_{dl} (nF)	R_p (k Ω)	Q_p (nF)
MgZnMn	19,054.6	-1.694	92.89	1.34	3372	–	–
MgZnMn-PCL	1,625.5	-1.604	89.38	69.67	105.2	11.93	9.06
MgZnMn-PTMC	15.1	-1.478	90.12	363.2	83.88	27.78	0.36

magnitude lower than that of the uncoated MgZnMn, and one order lower than that of the PCL-coated MgZnMn. From the thermodynamic point of view, E_{corr} of the PTMC-coated MgZnMn is higher than that of the uncoated and the PCL-coated MgZnMn by 216 mV and 90 mV, respectively. After the corrosion test, SEM imaging of the surface of the PTMC-coated MgZnMn revealed an intact, smooth and homogeneous surface, whereas some micropores were visible on the PCL-coated MgZnMn as well as a number of serious and large corrosive caverns on the surface of the MgZnMn sample (Supplementary materials, Fig. S3).

Corrosion mechanisms amongst the three samples were analyzed by EIS spectra and presented in Nyquist mode. Corresponding equivalent circuits for data fitting were developed and schematically inserted in EIS plots (Fig. 4b). The EIS response of the uncoated MgZnMn alloy can be fit with one time constant (Fig. 4b, inset), and modeled with the following components: where R_s , the testing solution resistance, is in series with a parallel circuit consisting of R_{ct} and Q_{dl} , the reaction resistance associated with interfacial charge transfer reaction process and capacitance

associated with the electrolyte double layer established at the interface, respectively. This circuit is denoted $R_s(Q_{\text{dl}} R_{\text{ct}})$. Addition of the polymer coating and EIS analysis reveal spectra described by two time constants (Fig. 4b). However, the PCL and PTMC polymers undergo different degradation pathways and thus the equivalent circuit models differed for the two samples. For the PTMC-coated MgZnMn, a model of $R_s(Q_{\text{dl}} R_{\text{ct}})(Q_p R_p)$ was employed to fit the data, where R_p and Q_p are identified as the resistance and capacitance pertaining to the polymer coating, respectively. The model of $R_s(Q_{\text{dl}}(R_{\text{ct}}(Q_p R_p)))$ was more suitable for the PCL-coated MgZnMn EIS response due to the fact that the bulk erosion of the PCL coating and the Mg alloy substrate corrosion are likely to occur simultaneously.

The fitted parameters of the impedance spectra are summarized in Table 1. The value of the reaction resistance R_{ct} is characteristic of the corrosion resistance of the polymer coatings and is worth comparing to determine the relative protective effect of each polymer. The R_{ct} value of the PTMC-coated MgZnMn is over two orders of magnitude larger than that of the uncoated MgZnMn sample and

over one order of magnitude larger than that the R_{ct} value of the PCL-coated MgZnMn. The modeled resistance of the PTMC coating, R_p , was also substantially higher, indicating an impeding effect on corrosion of the MgZnMn interpreted to be due to the protection of the PTMC coating acting as an ion conduction barrier. EIS analysis of the electrochemical corrosion testing suggests that PTMC coating is a superior protective barrier for the MgZnMn alloy in terms of corrosion resistance in dynamic m-SBF solution as compared to PCL coating.

3.2. In vitro hemocompatibility

3.2.1. Hemolysis ratio

The hemolysis ratio (HR) is widely used to evaluate the destructive degree of any implant material to erythrocytes. As shown in Table 2, the HR value of the PTMC- and PCL-coated samples were both within the 0.01–0.04% range, slightly lower than that of 316L SS (~0.26%), which served as a standard reference and control. The uncoated MgZnMn alloys had the highest HR of ~2.4%, although this value is still acceptable for clinical applications (<5%) [42].

3.2.2. Static platelet incubation

Platelet adhesion is a common indicator to evaluate hemocompatibility of blood-contacting materials [43]. The shape of platelet adherent on foreign materials can be classified in five categories and are listed in order of increased activation: round, dendritic, spread dendritic, spreading and fully spreading [44]. As shown in Fig. 5, there was a large number of adherent platelets on the 316L SS surface, and most were adhered, aggregated and activated to the extent of fully spreading state. By contrast, an extremely small number of platelets adhered on the MgZnMn surface, and those observed are still in the round state, i.e., no spreading as activation sign. It is noteworthy that substantial cracks developed on the MgZnMn surface, which can accelerate corrosion. In the case of PCL coating, a large number of platelets adhered on the PCL-coated MgZnMn surface (only slightly fewer than that of 316L SS), and they were activated to the extent of dendritic spreading state in the pseudo-podium stage (not as severely aggregated as 316L SS). However, a significantly lower amount of non-activated platelets in the natural state were observed on the PTMC-coated MgZnMn surface as compared to those on the 316L SS and PCL surface.

3.2.3. Human whole blood adhesion experiments in flow chamber

A dynamic whole blood adhesion experiment was conducted to monitor more realistically interactions between blood and the tested materials in vitro. A modified flow chamber for human whole blood adhesion experiments was designed (Supplementary material 1). On the 316L SS surface, the spreading dendritic platelets were clearly visible (Fig. 6a, green arrow), and some erythrocytes adhered on activated platelets (Fig. 6a, yellow arrow). On the MgZnMn surface, no visible platelet spreading occurred, but

Table 2
Hemolysis ratio of the samples: 316L SS, MgZnMn, PCL-coated MgZnMn, PTMC-coated MgZnMn (the size of substrate: $\varnothing 10$ mm \times 1.5 mm).

Sample	Hemolysis ratio (%)
316L SS	0.26 \pm 0.14
MgZnMn	2.41 \pm 0.24***
MgZnMn–PCL	0.01 \pm 0.17
MgZnMn–PTMC	0.04 \pm 0.14

Data expressed as mean \pm standard deviation (SD) and analyzed using a two-way ANOVA.

*** $p < 0.001$ compared to the three other samples, $N = 4$.

hemolysis reactions with some acanthocytes [45,46] formation occurred, and some of the erythrocytes were amoeboid without erythrocytosis (Fig. 6b, yellow arrow), which is consistent with the result of the hemolysis ratio. Some erythrocytes attached on the top of platelets as an activation process. Hemolysis reactions, blood coagulation and cracks formation all happened on the surface of the PCL-coated MgZnMn. As seen in Fig. 6c (yellow arrows), typical mutative morphologies of erythrocytes in the hemolysis reaction process were present, and most of adherent erythrocytes were aggregated. In addition, the degradation caused cracks on the PCL coating (Fig. 6c, green arrow). However, no hemolysis reactions, coagulation or cracks were observed on the surface of the PTMC-coated MgZnMn. There were not any adherent platelets and only few normal erythrocytes on it (Fig. 6d).

3.3. In vivo animal study

3.3.1. Biodegradable behavior in the tissue

For a further evaluation of the biodegradation, samples were implanted subcutaneously in rats for up to 16 and 52 weeks. The thicknesses of the PTMC and PCL coatings were both 10 ± 0.3 μ m before the implantation (Fig. 7a and b). After 16 weeks' implantation, optical evaluation of the specimens indicated no significant differences in the extent of degradation for the uncoated, the PCL- and PTMC-coated MgZnMn implants (Fig. 54). The degradation rate in subcutaneous tissue was slower than that in vitro.

Microtopographies of the 16-week implants generated by SEM of the implant–tissue interface, however, showed some remarkable diversity of the degradation degree. There were many potholes and cracks on the surface of the MgZnMn, and some exfoliation signs of the corrosion products emerged (Fig. 7c). Cracks extending hundreds of micrometers on the surface of the MgZnMn coated by the PCL were observed (Fig. 7d). The surface morphology of the MgZnMn coated by the PTMC presented excellent integrity and relative smoothness (Fig. 7e). The cross-section morphology observations are in agreement with the degradation degree analysis. There were many corrosive potholes and a corrosion layer with a thickness of 50–80 μ m between the MgZnMn and the tissue (Fig. 7f and i). The corrosion layer was loose because corrosion products peel off during rinsing of the antiscuffing paste (Fig. 7i, arrow). Similar characteristics were observed at the interface between the PCL-coated MgZnMn and the tissue. No continuous PCL coating was found (Fig. 7g and j). It is noteworthy that the local corrosion of the PCL-coated MgZnMn was more severe than the uncoated MgZnMn, and the thickness of the local corrosion layer exceeded 100 μ m, indicative of an accelerated corrosion of the Mg alloy. In contrast, the remaining PTMC coating is observed to have a thickness of 5–6 μ m, uniform and intact. Its thickness was reduced by ~45%, compared with that of pre-implantation (Fig. 7h and k).

CT-Xray analysis was performed on sample explants at 16 and 52 weeks to characterize the degradation process. The cross-sections and 3-D models of the implants were visualized after conducting the reconstructions (Fig. 8). For the 16-week implants, the obvious corrosion interfaces were observed on both the uncoated and PCL-coated MgZnMn (Fig. 8a and b). But a relatively smooth surface (green arrow) with a slight corrosion (yellow arrow) emerged on the PTMC-coated sample (Fig. 8c). The volume reductions of the uncoated, PCL-coated and PTMC-coated MgZnMn were ~15%, ~30% and ~7%, respectively. For the 52-week implants, a lot of corrosion products with some clear cracks were observed on the uncoated sample (Fig. 8d, yellow arrow), and the PCL-coated one was in distinct pieces due to significant degradation (Fig. 8e). Some areas of the PTMC-coated sample also incurred corrosion (Fig. 8f). The volume reductions of the uncoated, PCL-coated and PTMC-coated MgZnMn were ~33%, ~52% and ~22%, respectively. Corrosion products occupied ~35%, ~38% and ~11% of the total

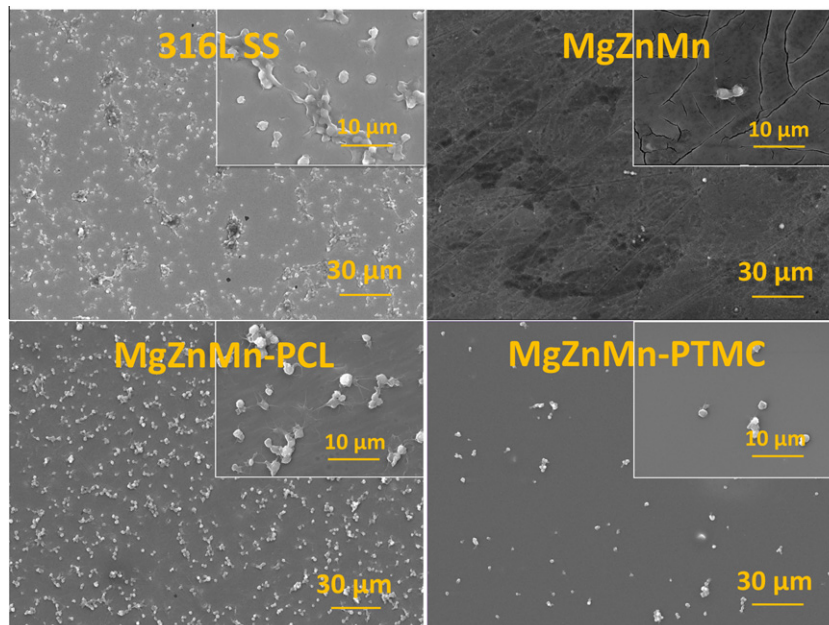


Fig. 5. Representative SEM images of adherent platelets on the surfaces of the samples: 316L SS, uncoated, PCL-coated and PTMC-coated MgZnMn samples incubated in PRP for 2 h.

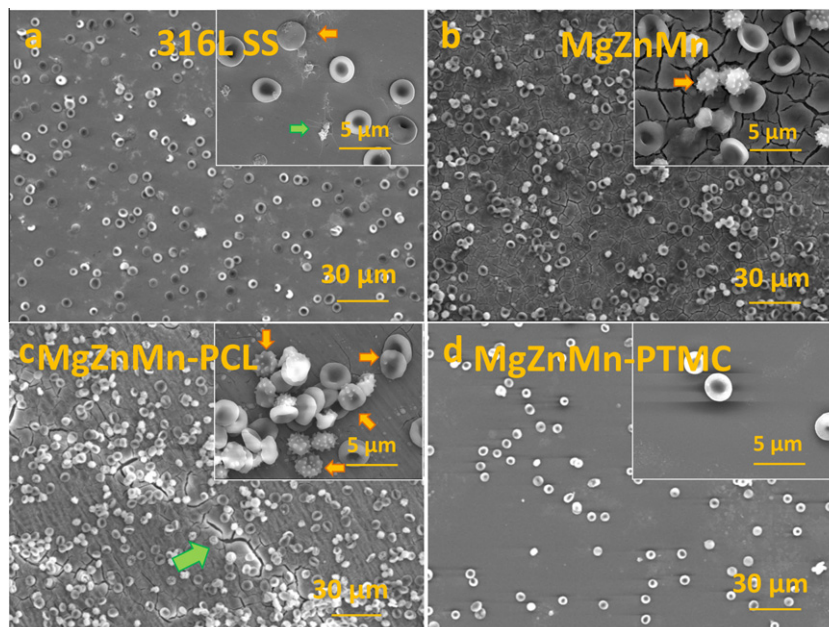


Fig. 6. Representative SEM images of samples: 316L SS, uncoated, PCL-coated and PTMC-coated MgZnMn samples in a flow chamber experiments in human whole blood for 2 h.

volume of the corroded uncoated, PCL-coated and PTMC-coated samples, respectively. Thus, the PTMC-coated MgZnMn had the least volume reduction and fewest corrosion products among all the samples.

3.3.2. Histological evaluation

The histological evaluation of the tissue response to these implants was carried out qualitatively. The analysis of the 16-week implantation of the uncoated, PCL-coated and PTMC-coated MgZnMn samples had neither induced any local toxic effect nor caused any obvious local response of the tissue. From macroscopic evaluation of the implant sites of the specimens, there were no sig-

nificant signs of inflammation, encapsulation, hemorrhage, necrosis or discoloration. But a few differences between the PCL-coated MgZnMn and the uncoated/PTMC-coated one were observed from microscopic evaluation. For the uncoated and PTMC-coated MgZnMn samples, only a fibrocyte monolayer exists at the implant–tissue interface. For the PCL-coated MgZnMn sample, there was a thicker fibrous capsule ($\sim 40 \mu\text{m}$) and a small number of macrophages and plasmocytes in the surrounding region with a slight inflammation response (Fig. 9). No gas bubbles were observed in the surrounding tissue to the naked eye or histological analysis in all samples. Overall, PTMC-coated MgZnMn sample displayed an excellent tissue response.

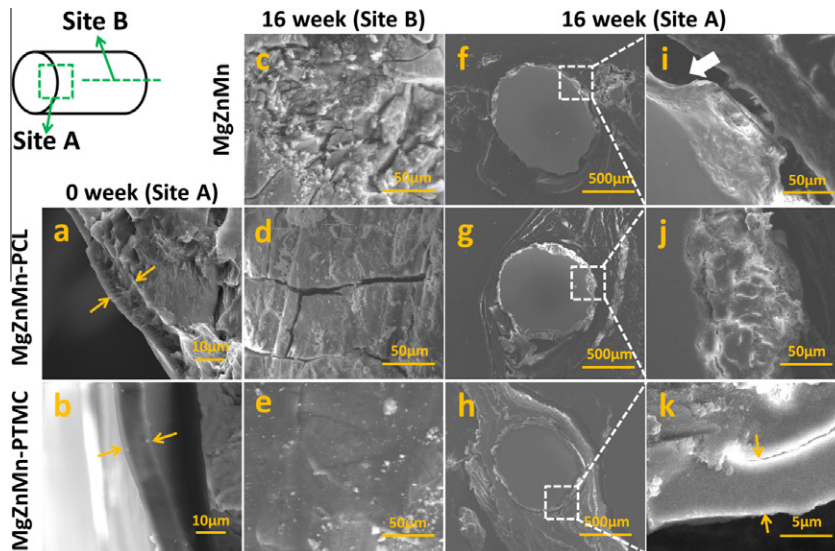


Fig. 7. SEM micrographs characterizing the in vivo degradation behavior of the implants after 16 weeks. In schematic inset, site A is an interface between the metal wire and the tissue/polymer in the cross-section; site B is a surface of the metal along the axis of the metal wire, after removing the tissue and polymer. Representative SEM images of samples: the site A of PCL-coated (a) and PTMC-coated (b) MgZnMn wires in the pre-implantation (0 week); the site B of uncoated (c), PCL-coated (d) and PTMC-coated (e) MgZnMn wires after 16 weeks implantation; the site A of uncoated (f and i), PCL-coated (g and j) and PTMC-coated (h and k) MgZnMn wires after 16 weeks implantation. Yellow arrows indicate polymer coating.

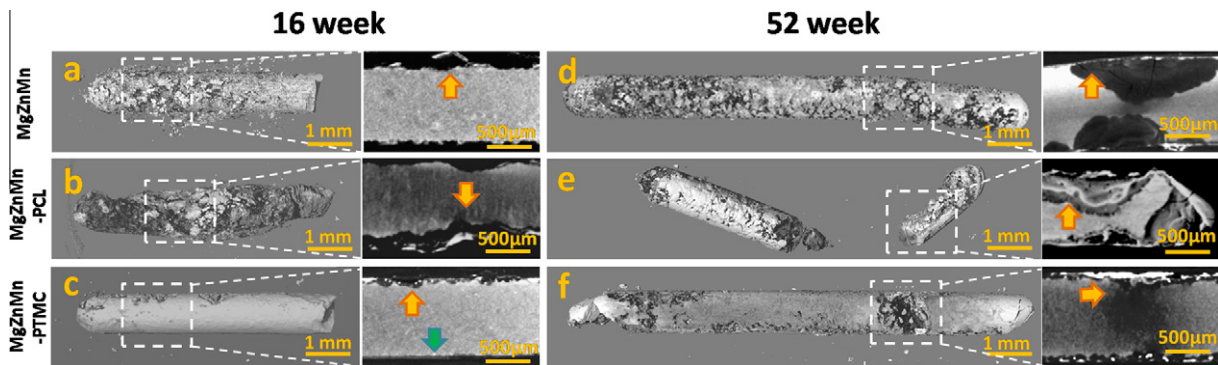


Fig. 8. Reconstructions of X-ray nano-CT 3-D with representative 2-D slices of the uncoated (a and d), PCL-coated (b and e) and PTMC-coated (c and f) samples after 16 and 52 weeks implantation, respectively. (One part of samples for 16 weeks are shown after brittle fracture, and the complete samples for 52 weeks are shown.) Yellow arrows indicate corrosion products, and green arrow indicate a smooth interface between the implant and the surrounding tissue.

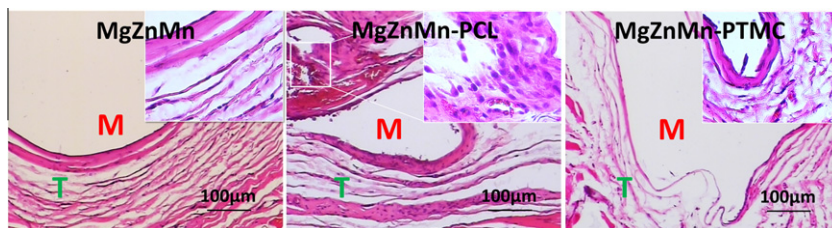


Fig. 9. Micrographs of the histological analysis of the implants after 16 weeks post-operation: uncoated, PCL-coated and PTMC-coated MgZnMn. M regions represent the implants; T regions represent the tissue.

4. Discussion

4.1. Biodegradation mechanism

4.1.1. The influence of degradation behavior of the polymer coating on the Mg alloy corrosion

Intuitively, there are many polymer coatings that are likely to provide a barrier to Mg alloy corrosion. Typically, however, the

polymeric barrier is effective only in the short term [36,47]. In fact, the degradation behavior of the polymer coating itself may play a crucial role in the subsequent corrosion of Mg substrate. In our case, PTMC is determined to degrade uniquely in a surface-eroding mode and thus is advantageous for corrosion control of Mg alloy in the longer term.

The hydrolytic degradation of polymer coatings can be described as a trade-off between hydrolysable bond cleavage and

water uptake process [48]. Depending on the ratio for the time constants of water uptake and bond cleavage, two basic degradation modes exist, namely surface erosion and bulk erosion. For surface eroding polymer, the cleavage of critical bonds is considerably faster than water uptake [49], leading to a linear mass loss during erosion [50,51]. In such cases, surface degradation proceeds at the interface between the polymeric specimens and the aqueous environment [37], and a decrease in molecular weight is negligible during the whole degradation [49]. A few kinds of polymers like PTMC are surface-eroding, such as certain polycarbonates, polyanhydrides and polyorthoesters. In contrast, for bulk-eroding polymers, the uptake of water is considerably faster than critical bond splitting. This leads to the effect that polymer is first completely soaked with a certain amount of water before actual degradation starts throughout the bulk, and the molecular weight persistently decrease during the whole degradation [49]. Most of biodegradable polymeric materials studied in the literature, such as PLA, PLGA and PCL, predominantly present such bulk degradation [52]. Actually, they may be not long-term effective for surface modification of Mg-based materials.

Our degradation results showed that PTMC on Mg alloy was indeed homogeneously thinned from the surface to the interior when exposed to biologically relevant environments. Therefore, Mg alloy can be well protected and packaged by the coating for at least for 1 month in the dynamic degradation assay in vitro (Fig. 21) and even longer, for up to 16 and 52 weeks in vivo (Figs. 7 and 8). These observations are consistent with the natural corrosion current I_{corr} , which is decreased over three orders of magnitude after coating with PTMC (Fig. 4a). Surface-eroding PTMC offers an electrochemically inert outer layer. The PTMC surface-eroding degradation process helps to maintain an intact residual layer during degradation of the outer layer(s), providing a protective pathway to impede electrolyte diffusing from blood to the Mg alloy and thus substrate corrosion is minimized (Fig. 3e and f). In contrast, bulk-eroding PCL produced a number of micro- and even macropores and cracks in early stage of the degradation, exposing the Mg substrate directly to blood (Fig. 6c). Electrical diffusion pathway is thus readily formed between blood and Mg alloy on the exposed sites and further accelerates corrosion of Mg alloy, as schematically illustrated in Fig. 10.

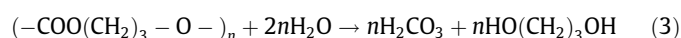
4.1.2. The influence of degradation products of the polymer coating on the Mg alloy corrosion

Another key factor for Mg corrosion protection is the chemical interplay between the degradation products of coating and Mg substrate. PTMC hydrolysis is an approximately net neutral ionic process and tends to maintain a physiological pH during degradation. This feature is distinguishable from other commonly chosen polymers for implant corrosion protection.

Many biodegradable polymer coatings like PCL actually enhance the corrosion rate of Mg alloy [36], because they degrade by the hydrolysis of their ester bonds and release carboxylic acids to the local environment [38]. Additionally, once the alloy is exposed to

corrosive environment, due to breaching of the polymeric barrier, the corrosion of Mg alloy produces a locally alkaline environment and some products such as $\text{Mg}(\text{OH})_2$ can accelerate the hydrolysis rate of the polymer, and the stability of PCL coating is weakened further. Meanwhile, the acidic products from the PCL hydrolysis can react with the Mg corrosion products such as $\text{Mg}(\text{OH})_2$ and the metallic substrate under aqueous conditions. The synergy of these degradation phenomena result in accelerated corrosion in the PCL coated Mg system. Ultimately the integrity and functionality of the PCL coating collapses under the dual effects of the evolved H_2 and dissolved $\text{Mg}(\text{OH})_2$ in the free diffusing solution.

In contrast, the PTMC hydrolysis is approximately neutral, and it degrades enzymatically in vivo by surface erosion without releasing any strong acidic compounds such as polylactic acid (PLA) [49], according to the formula:



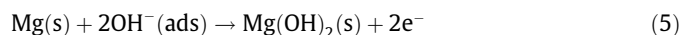
Because of the slow degradation and the surface eroding behavior of PTMC, the degradation products are kept away from the Mg substrate and have minimal effect on the corrosion of the Mg alloy, in contrast to the acidic degradation products of bulk eroding polymer PCL coating, which accelerates the Mg corrosion process.

It has been demonstrated that the interface of PTMC coating remains intact and clear in all experiment environments tested in this study (Fig. 3e and f), indicating polymeric stability at least at the micron scale. In fact, the biodegradable PTMC polymer does not offer complete non-permeable coverage. PTMC does allow a small amount of electrolyte penetration through the coating to react with the Mg alloy substrate underneath. Notably, the corrosion only occurred on the surface of the metallic substrate, and PTMC coating did not participate overtly in this process. In the confined environment, two possibilities of Mg corrosion near metallic surface intimately covered by PTMC are considered:

- (i) Commonly the corrosion of Mg is described according to the following [53]:



In the case of PTMC coating, the diffusion of H_2O through the coating is severely limited, thus this is not considered to be the major corrosion pathway. (ii) Another explanation may be more plausible due to the size and mobility of H^+ and OH^- present in the solution [54]. For the formation of $\text{Mg}(\text{OH})_2$ the pH will not change as the same amount of H^+ and OH^- are used, according to Eqs. (5) and (6):



No visible bulging of the complete PTMC coatings and hydrogen bubbles was observed on the PTMC-coated MgZnMn during the whole degradation. Adsorbed hydrogen ions receive electrons, and form hydrogen atoms which then react with Mg, forming MgH_2 according to Eqs. (6) and (7):

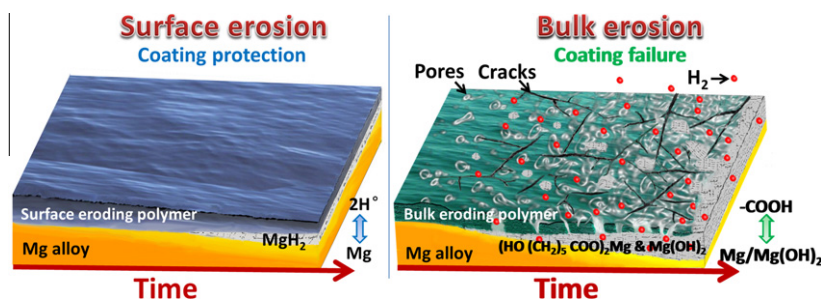
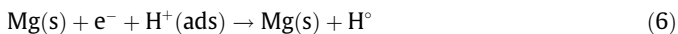


Fig. 10. Schematic diagram of surface and bulk erosion as a function of time.



Regardless of the product layer is Mg(OH)_2 or MgH_2 , the remaining PTMC maintains the stability of this thin corrosion layer, and prevents further dissolution and corrosion. Furthermore, the remaining PTMC coupled with this thin corrosion layer causes an enhanced diffusion barrier, and the overall degradation process is slowed down in the confined environment [15], as schematically illustrated in Fig. 10.

The kinetic factors are mainly determinants for highly corrosive Mg alloy and depend on the rate-determining step (RDS) of overall corrosion process [53]. The EIS measurements offer some insight into the pathways for Mg corrosion of the coated substrates. On the uncoated MgZnMn alloy, the RDS could be the corrosion reaction itself, as illustrated by R_{ct} . For surface-modified Mg alloy, the RDS is likely to be an electrolyte diffusion through microchannels in coating, indicated by the resistance related to polymer R_p , which therefore in turn causes a slower Mg corrosion reaction (i.e. larger R_{ct}) than that of the uncoated alloy. The RDS herein depends on the developing surface/interface states influenced by molecular transportation, absorption, desorption and products formation. For PTMC-coated MgZnMn, the RDS is closely determined by the water/ion/electrolyte penetration through the coating to the MgZnMn substrate. In the case of PTMC coated alloys, this rate remains very low due to uniform thinning of coating. For bulk-eroding PCL polymer coatings, the mechanism of corrosion is more complex as there are many micro/macro pathways allowing water to reach the substrate.

4.2. Hemocompatibility

Good hemocompatibility involves not only no hemolysis but also no coagulation. Rapid corrosion rate of Mg can lead to high pH, which is associated with high HR [55]. In this present study, only MgZnMn alloy induced a slight hemolysis reaction. In the dynamic human whole blood tests, the uncoated and PCL-coated MgZnMn alloys both presented erythrocytopenia, but not erythrorrhesis. It can be seen that the corrosion rate in the whole blood is higher than that in 0.9% (w/v) sodium chloride solution used in the hemolysis ratio test. Mg release in human whole blood was 10 times higher than that in PBS under static conditions [56]. Due to the fast degradation, nearly one third of erythrocytes showed erythrocytopenia and abnormally shaped acanthocytes on the MgZnMn alloys, and the cracked PCL coating allows the corrosion of the Mg substrate concomitant with the hemolysis reaction. However, PTMC did not cause hemolysis itself, and it also offered a stable protective layer to prevent the hemolysis caused by the corrosion of the Mg substrate.

The inhibition of thrombosis is a priority for blood contacting materials. Activated platelets trigger the coagulation of blood leading to thrombus formation [57]. The uncoated and PTMC-coated MgZnMn both have favorable anti-coagulant properties. In the intrinsic or extrinsic pathways of the coagulation cascade, calcium ions are essential for the coagulation process [58]. The enhanced release of Mg^{2+} during the rapid corrosion process destroys the equilibrium between Ca^{2+} and Mg^{2+} bound to proteins [59]. A high Mg^{2+} concentration may inhibit plasma-coagulation cascade. As reported, introduction of Mg^{2+} via intravenous, continuous infusion route or boluses inhibits platelet aggregation only at high doses [60]. According to the activated partial thromboplastin time (aPTT), prothrombin time (PT) and thrombin time (TT) blood coagulation assays (Supplementary Materials 5), the aPTT of the MgZnMn surface was 47.1 s longer than that of control original plasma (31.4 s), and their PT and TT are also prolonged relative to that of control sample, indicating that activation of the intrinsic and extrinsic

blood coagulation system was effectively suppressed on the MgZnMn surface. This result is attributed to high Mg^{2+} concentration released by the local corrosion. In addition, owing to the rapid surface degradation, Mg alloy cannot provide a stable interface for platelet adhesion. These mechanisms are further confirmed by our static platelet incubation and dynamic whole blood tests.

On the other hand, rapid adsorption of plasma proteins occurs on the exogenous surface, which leads to platelet adhesion and triggers the coagulation of blood leading to thrombus formation [57]. The adhesion and activation of platelets mainly depend on the surface nature of the materials and the adsorbed proteins [57]. The amount and conformation of the adsorbed fibrinogen are the key factors that determine the response of platelets to materials [61,62]. For the PCL surface, most activated platelets and adherent erythrocytes were aggregated, because the PCL may denature the adsorbed fibrinogens that snare a number of platelets and erythrocytes. On the PTMC surface, almost all platelets and erythrocytes were in their resting state and did not aggregate, suggesting intact fibrinogens on the PTMC surface.

4.3. Histocompatibility

In vivo biocompatibility tests are crucial because they assess the local effects of a material or implant device in contact with living tissue. According to our results, the uncoated and PTMC-coated MgZnMn are both acceptable with mild tissue reaction by clinical standards. Good tissue compatibility of Mg alloy is a prime factor for promotion of this material as stent candidates of the future [4]. PTMC polymer shows good biocompatibility in terms of long-term cytotoxicity, irritation, mutation and sensitization tests [63]. The PTMC-coated MgMnZn sample exhibits an excellent tissue response, probably due to its slow degradation rate and neutral degradation products [64–66]. However, the PCL-coated MgMnZn sample produces a high quantity of acidic degradation products in a short time and induces a slight inflammatory response [38]. This study shows that a slow release and low amount of PTMC degradation products are better tolerated in tissue than the higher and more acidic release associated with the degradation of PCL.

Accordingly, an ideal coating for Mg alloys to achieve a desirable period of implantation should be designed through the following optimizations:

- (i) suitable biodegradation behavior of the coating;
- (ii) well-matched chemical interaction between the coating and the Mg substrate during the degradation;
- (iii) good biocompatibility of the coating such as hemocompatibility, cytocompatibility, and histocompatibility.

From the comprehensive performances summarized in Table 3, the PTMC-coated MgZnMn alloy presents good corrosion resistance, less to no hemolytic reaction, less coagulation and better tissue compatibility with a mild response than the controls tested.

5. Conclusion

We have demonstrated a surface eroding coating, PTMC, that provides a route for improvement in both the durability and biocompatibility of Mg-based stents. Different from the cavernous corrosion behavior of conventional bulk-eroding polymers, the homogeneous surface erosion of the PTMC coating from exterior to interior can effectively protect the Mg-based substrate both in vitro and in vivo. The neutral degradation products of the PTMC coating provide a mild microenvironment that neither accelerates the corrosion of Mg alloy nor triggers inflammation on the surrounding tissue in comparison with acidic byproducts of associated

Table 3

Comparison of uncoated, PCL-coated and PTMC-coated MgZnMn samples for biodegradation behavior, hemocompatibility and histocompatibility.

Sample	Property			Histocompatibility
	Biodegradation behavior	Hemocompatibility		
		Hemolysis	Coagulation	
MgZnMn	–	±	+	+
MgZnMn–PCL	–	+	–	±
MgZnMn–PTMC	+	+	+	+

“–” represents bad performance; “±” represents acceptable performance; “+” represents good performance.

with commonly used biopolymers such as PCL. The PTMC coated MgZnMn also shows good hemocompatibility, including low hemolytic ratio and low coagulation. This study offers a promising approach for the development of fully biodegradable cardiovascular stents.

Acknowledgements

The authors would like to thank Dr Zhihao Yuan, Dr Donghui Zhu, Dr Zhilu Yang and Dr Jialong Chen for their help and valuable discussions. This study was supported by the National Natural Science Foundation of China under Grant Nos. 81271701 and 20973134, Key Basic Research Program of China 2011CB606204, China Scholarship Council 201207000016, Sichuan Youth Science & Technology Foundation (No. 2012JQ0001) for Distinguished Young Scholars and Engineering Research Center for Revolutionizing Metallic Biomaterials (NSF-0812348) from the National Science Foundation.

Appendix A. Figures with essential color discrimination

Certain figures in this article, particularly Figs. 1–10, are difficult to interpret in black and white. The full color images can be found in the on-line version, at <http://dx.doi.org/10.1016/j.actbio.2013.02.041>

Appendix B. Supplementary data

Supplementary data associated with this article can be found, in the online version, at <http://dx.doi.org/10.1016/j.actbio.2013.02.041>.

References

- [1] Savage MP, Fischman DL, Schatz RA, Leon MB, Baim DS, Brinker J, et al. Coronary intervention in the diabetic patient: improved outcome following stent implantation compared with balloon angioplasty. *Clin Cardiol* 2002;25:213–7.
- [2] Erne P, Schier M, Resink TJ. The road to bioabsorbable stents: reaching clinical reality? *Cardiovasc Intervent Radiol* 2005;29:11–6.
- [3] Colombo A, Karvouni E. Biodegradable stents: “fulfilling the mission and stepping away”. *Circulation* 2000;102:371–3.
- [4] Moravej M, Mantovani D. Biodegradable metals for cardiovascular stent application: interests and new opportunities. *Int J Mol Sci* 2011;12:4250–70.
- [5] Mani G, Feldman MD, Patel D, Agrawal CM. Coronary stents: a materials perspective. *Biomaterials* 2007;28:1689–710.
- [6] Erne P, Schier M, Resink TJ. The road to bioabsorbable stents: reaching clinical reality? *Cardiovasc Intervent Radiol* 2006;29:11–6.
- [7] Witte F, Hort N, Vogt C, Cohen S, Kainer KU, Willumeit R, et al. Degradable biomaterials based on magnesium corrosion. *Curr Opin Solid State Mater Sci* 2008;12:63–72.
- [8] Witte F. The history of biodegradable magnesium implants: a review. *Acta Biomater* 2010;6:1680–92.
- [9] Yun Y, Dong Z, Lee N, Liu Y, Xue D, Guo X, et al. Revolutionizing biodegradable metals. *Mater Today* 2009;12:22–32.
- [10] Atrens A, Liu M, Zainal Abidin NI. Corrosion mechanism applicable to biodegradable magnesium implants. *Mater Sci Eng B* 2011;176:1609–36.
- [11] Saris N-EL, Mervaala E, Karppanen H, Khawaja JA, Lewenstam A. Magnesium: an update on physiological, clinical and analytical aspects. *Clin Chim Acta* 2000;294:1–26.
- [12] Staiger MP, Pietak AM, Huadmai J, Dias G. Magnesium and its alloys as orthopedic biomaterials: a review. *Biomaterials* 2006;27:1728–34.
- [13] Gray JE, Luan B. Protective coatings on magnesium and its alloys – a critical review. *J Alloys Compd* 2002;336:88–113.
- [14] Yamamoto A, Watanabe A, Sugahara K, Tsubakino H, Fukumoto S. Improvement of corrosion resistance of magnesium alloys by vapor deposition. *Scr Mater* 2001;44:1039–42.
- [15] Witte F, Kaese V, Haferkamp H, Switzer E, Meyer-Lindenberg A, Wirth CJ, et al. In vivo corrosion of four magnesium alloys and the associated bone response. *Biomaterials* 2005;26:3557–63.
- [16] Zberg B, Uggowitz PJ, Loeffler JF. MgZnCa glasses without clinically observable hydrogen evolution for biodegradable implants. *Nat Mater* 2009;8:887–91.
- [17] Gu X, Zheng Y, Cheng Y, Zhong S, Xi T. In vitro corrosion and biocompatibility of binary magnesium alloys. *Biomaterials* 2009;30:484–98.
- [18] Hornberger H, Virtanen S, Boccaccini AR. Biomedical coatings on magnesium alloys – a review. *Acta Biomater* 2012;8:2442–55.
- [19] Wu G, Ibrahim JM, Chu PK. Surface design of biodegradable magnesium alloys – a review. *Surface and Coatings Technology*.
- [20] Gu XN, Li N, Zhou WR, Zheng YF, Zhao X, Cai QZ, et al. Corrosion resistance and surface biocompatibility of a microarc oxidation coating on a Mg–Ca alloy. *Acta Biomater* 2011;7:1880–9.
- [21] Zhang XP, Zhao ZP, Wu FM, Wang YL, Wu J. Corrosion and wear resistance of AZ91D magnesium alloy with and without microarc oxidation coating in Hank's solution. *J Mater Sci* 2007;42:8523–8.
- [22] Yao Z, Li L, Jiang Z. Adjustment of the ratio of Ca/P in the ceramic coating on Mg alloy by plasma electrolytic oxidation. *Appl Surf Sci* 2009;255:6724–8.
- [23] Blawert C, Dietzel W, Ghalil E, Song G. Anodizing treatments for magnesium alloys and their effect on corrosion resistance in various environments. *Adv Eng Mater* 2006;8:511–33.
- [24] Hiromoto S, Yamamoto A. Control of degradation rate of bioabsorbable magnesium by anodization and steam treatment. *Mater Sci Eng C* 2010;30:1085–93.
- [25] Gu XN, Zheng W, Cheng Y, Zheng YF. A study on alkaline heat treated Mg–Ca alloy for the control of the biocorrosion rate. *Acta Biomater* 2009;5:2790–9.
- [26] Pereda MD, Alonso C, Burgos-Asperilla L, del Valle JA, Ruano OA, Perez P, et al. Corrosion inhibition of powder metallurgy Mg by fluoride treatments. *Acta Biomater* 2010;6:1772–82.
- [27] Drynda A, Hassel T, Hoehn R, Perz A, Bach F-W, Peuster M. Development and biocompatibility of a novel corrodible fluoride-coated magnesium–calcium alloy with improved degradation kinetics and adequate mechanical properties for cardiovascular applications. *J Biomed Mater Res Part A* 2010;93A:763–75.
- [28] Wang HX, Guan SK, Wang X, Ren CX, Wang LG. In vitro degradation and mechanical integrity of Mg–Zn–Ca alloy coated with Ca-deficient hydroxyapatite by the pulse electrodeposition process. *Acta Biomater* 2010;6:1743–8.
- [29] Xu L, Zhang E, Yang K. Phosphating treatment and corrosion properties of Mg–Mn–Zn alloy for biomedical application. *J Mater Sci Mater Med* 2008;20:859–67.
- [30] Sealy MP, Guo YB. Surface integrity and process mechanics of laser shock peening of novel biodegradable magnesium–calcium (Mg–Ca) alloy. *J Mech Behav Biomed Mater* 2010;3:488–96.
- [31] Wu GS, Xu RZ, Feng K, Wu SL, Wu ZW, Sun GY, et al. Retardation of surface corrosion of biodegradable magnesium-based materials by aluminum ion implantation. *Appl Surf Sci* 2012;258:7651–7.
- [32] Salunke P, Shanov V, Witte F. High purity biodegradable magnesium coating for implant application. *Mater Sci Eng B Adv Funct Solid State Mater* 2011;176:1711–7.
- [33] Wong HM, Yeung KWK, Lam KO, Tam V, Chu PK, Luk KDK, et al. A biodegradable polymer-based coating to control the performance of magnesium alloy orthopaedic implants. *Biomaterials* 2010;31:2084–96.
- [34] Gu XN, Zheng YF, Lan QX, Cheng Y, Zhang ZX, Xi TF, et al. Surface modification of an Mg–1Ca alloy to slow down its biocorrosion by chitosan. *Biomed Mater* 2009;4.
- [35] Gray-Munro JE, Seguin C, Strong M. Influence of surface modification on their vitro corrosion rate of magnesium alloy AZ31. *J Biomed Mater Res Part A* 2009;91A:221–30.
- [36] Chen Y, Song Y, Zhang S, Li J, Zhao C, Zhang X. Interaction between a high purity magnesium surface and PCL and PLA coatings during dynamic degradation. *Biomed Mater* 2011;6:025005.

- [37] Hofmann D, Entrialgo-Castaño M, Kratz K, Lendlein A. Knowledge-based approach towards hydrolytic degradation of polymer-based biomaterials. *Adv Mater* 2009;21:3237–45.
- [38] Taylor MS, Daniels AU, Andriano KP, Heller J. Six bioabsorbable polymers: in vitro acute toxicity of accumulated degradation products. *J Appl Biomater* 1994;5:151–7.
- [39] Chen Y, Zhang S, Li J, Song Y, Zhao C, Zhang X. Dynamic degradation behavior of MgZn alloy in circulating m-SBF. *Mater Lett* 2010;64:1996–9.
- [40] Doriot PA, Dorsaz PA, Dorsaz L, De Benedetti E, Chatelain P, Delafontaine P. In vivo measurements of wall shear stress in human coronary arteries. *Coron Artery Dis* 2000;11:495–502.
- [41] Shi Z, Liu M, Atrens A. Measurement of the corrosion rate of magnesium alloys using Tafel extrapolation. *Corros Sci* 2010;52:579–88.
- [42] ISO/TR 7405–1984. Biological Evaluation of Dental Materials Contents, Heamolysis Test (In Vitro Test Directly on Materials) [e-documentation].
- [43] Goodman SL, Grasel TG, Cooper SL, Albrecht RM. Platelet shape change and cytoskeletal reorganization on polyurethaneureas. *J Biomed Mater Res* 1989;23:105–23.
- [44] McEver RP, Martin MN. A monoclonal antibody to a membrane glycoprotein binds only to activated platelets. *J Biol Chem* 1984;259:9799–804.
- [45] Ways P, Simon ER. The role of serum in acanthocyte autohemolysis and membrane lipid composition. *J Clin Invest* 1964;43:1322–8.
- [46] Kayden HJ, Bessis M. Morphology of normal erythrocyte and acanthocyte using Nomarski optics and the scanning electron microscope. *Blood* 1970;35:427–36.
- [47] Xu L, Yamamoto A. In vitro degradation of biodegradable polymer-coated magnesium under cell culture condition. *Appl Surf Sci* 2012;258:6353–8.
- [48] Vert M, Li S, Garreau H, Mauduit J, Boustta M, Schwach G, et al. Complexity of the hydrolytic degradation of aliphatic polyesters. *Angew Makromol Chem* 1997;247:239–53.
- [49] Zhang Z, Kuijjer R, Bulstra SK, Grijpma DW, Feijen J. The in vivo and in vitro degradation behavior of poly(trimethylene carbonate). *Biomaterials* 2006;27:1741–8.
- [50] Middleton JC, Tipton AJ. Synthetic biodegradable polymers as orthopedic devices. *Biomaterials* 2000;21:2335–46.
- [51] Kluin OS, van der Mei HC, Busscher HJ, Neut D. A surface-eroding antibiotic delivery system based on poly-(trimethylene carbonate). *Biomaterials* 2009;30:4738–42.
- [52] Tamada JA, Langer R. Erosion kinetics of hydrolytically degradable polymers. *Proc Natl Acad Sci U S A* 1993;90:552–6.
- [53] Song G, Atrens A, Stjohn D, Nairn J, Li Y. The electrochemical corrosion of pure magnesium in 1 N NaCl. *Corros Sci* 1997;39:855–75.
- [54] Hornberger H, Witte F, Hort N, Mueller WD. Effect of fetal calf serum on the corrosion behaviour of magnesium alloys. *Mater Sci Eng B* 2011;176:1746–55.
- [55] Bodansky M. The effect of hydrogen ion concentration on saponin hemolysis. *J Biol Chem* 1929;83:567–77.
- [56] Geis-Gerstorf J, Schille C, Schweizer E, Rupp F, Scheideler L, Reichel HP, et al. Blood triggered corrosion of magnesium alloys. *Mater Sci Eng B* 2011;176:1761–6.
- [57] Davie EW, Fujikawa K. Basic mechanisms in blood coagulation. *Annu Rev Biochem* 1975;44:799–829.
- [58] Vogler EA, Siedlecki CA. Contact activation of blood-plasma coagulation. *Biomaterials* 2009;30:1857–69.
- [59] Mayer MM, Osler AG, Bier OG, Heidelberger M. The activating effect of magnesium and other cations on the hemolytic function of complement. *J Exp Med* 1946;84:535–48.
- [60] Ravn HB, Kristensen SD, Hjortdal VE, Thygesen K, Husted SE. Early administration of intravenous magnesium inhibits arterial thrombus formation. *Arterioscler Thromb Vasc Biol* 1997;17:3620–5.
- [61] Nachman RL, Leung LL. Complex formation of platelet membrane glycoproteins IIb and IIIa with fibrinogen. *J Clin Invest* 1982;69:263–9.
- [62] Roach P, Farrar D, Perry CC. Interpretation of protein adsorption: surface-induced conformational changes. *J Am Chem Soc* 2005;127:8168–73.
- [63] Wójcik K, Verdoold V, Koopmans SA, de Vos SNV, Grijpma DW. In vivo application of poly(1,3-trimethylene carbonate) as a scleral buckle in a rabbit model. *Macromol Symp* 2011;309–310:68–75.
- [64] Fournier E, Passirani C, Montero-Menei CN, Benoit JP. Biocompatibility of implantable synthetic polymeric drug carriers: focus on brain biocompatibility. *Biomaterials* 2003;24:3311–31.
- [65] Edlund U, Albertsson AC. Copolymerization and polymer blending of trimethylene carbonate and adipic anhydride for tailored drug delivery. *J Appl Polym Sci* 1999;72:227–39.
- [66] Edlund U, Albertsson AC, Singh SK, Fogelberg I, Lundgren BO. Sterilization, storage stability and in vivo biocompatibility of poly(trimethylene carbonate)/poly(adipic anhydride) blends. *Biomaterials* 2000;21:945–55.